Nirav Annavarapu, Iakov Goldberg, Athina Papadopoulou, Karim Elkhouly, Jan Genoe, Robert Gehlhaar, and Paul Heremans. 2023. Scattered Emission Profile Technique for Accurate and Fast Assessment of Optical Gain in Thin Film Lasing Materials. *ACS Photonics* 10(5), 1583-1590. DOI: 10.1021/acsphotonics.3c00204

Scattered Emission Profile Technique for Accurate and Fast Assessment of Optical Gain in Thin Film Lasing Materials

Nirav Annavarapu[ab], Iakov Goldberg[ab], Athina Papadopoulou[ab], Karim Elkhouly[ab], Jan Genoe [ab], Robert Gehlhaar[a], Paul Heremans[ab*]*

Affiliations

[a]*imec, Kapeldreef 75, Leuven 3001, Belgium*
[b]*KU Leuven, ESAT department, Kasteelpark Arenberg 10, Leuven 3001, Belgium*
[*)]*Email: nirav.annavarapu@imec.be; paul.heremans@imec.be*

Abstract: Accurate measurement of optical gain is essential to screen materials as viable active media for thin-film laser applications. The net modal gain is typically measured using the variable stripe length (VSL) method, which has been extensively studied for the last few decades. In this work, we propose an alternative method, which we name scattered emission profile (SEP) method, to measure the net modal gain. It relies on the collection of amplified spontaneous emission (ASE) scattered from the surface of the film illuminated by a pump stripe. By using an appropriate setup, the new method results in a significantly faster measurement of net modal gain, while simultaneously providing a more accurate gain value. The setup and algorithm to extract the net modal gain are detailed in this paper and are demonstrated on Lead Halide Perovskite films. The influence of the stripe length on the measured gain value is shown. Gain measurements performed over two different perovskite films, fabricated either via spin-coating or thermal evaporation, confirm the broad applicability of the SEP method. Finally, we show a quantitative comparison of the SEP method with VSL measurements, and highlight the advantages and shortcomings of each method.

Keywords: Net modal gain; Optical gain measurement; Scattered emission profile; Lasing; Perovskite; Variable Stripe Length

Introduction

Thin-film materials such as Metal Halide Perovskites and Colloidal Quantum Dots have garnered a lot of research interest as active media for lasers[1–3]. Over the past decades, there have been numerous demonstrations of optically pumped lasing from these materials[4–9]. Simultaneously, there have also been several developments towards pushing high current densities into Light Emitting Diodes (LEDs), with the goal of achieving injection lasing[10–13]. Indeed, such thin-film injection lasers, when achieved, would eliminate a number of shortcomings of today's hetero-integrated lasers on chips[14], by enabling cost-effective processing, ease of manufacturing and lattice-independent substrate-compatibility. They can also allow to envisage new concepts, such as flexible lasers[15,16].

To study the performance of thin film materials as active media, several optical properties need to be quantified, such as their optical gain, amplified spontaneous emission (ASE) threshold, radiative recombination lifetime, etc. Characterization of optical gain is essential to benchmark and compare different materials as gain media, and to model the behavior of lasing structures using rate equations. Typically, optical gain is characterized using either transient absorption spectroscopy (TAS)[17] which provides information about the maximum intrinsic gain of the material, or the variable stripe length (VSL)[18–21] method, which measures the net modal gain of a material under optical pumping (or electrical pumping in the segmented-contact variant[22]). Both techniques have been studied for decades[23,24] and have been extensively used to measure

the gain for several material systems[21,25–29]. The value of the gain measured over these films depends heavily on the characterization technique. On the one hand, for a typical perovskite film, TAS measurements report intrinsic gain values as high as 2000-3200 cm^{-1} [28,29], which must be multiplied by the confinement factor of a mode to obtain the net modal gain. On the other hand, the VSL method directly measures the net modal gain after overcoming the scattering losses and is generally an important input parameter for simulation models of lasers. The net modal gain values obtained using the VSL technique depend heavily on the fitting model used[25] and on the pump fluence (with gains ranging from 50 cm^{-1} to 1000 cm^{-1} [26]).

The commonly used VSL method imposes strict requirements to get an accurate measurement. The pump stripe must be precisely aligned with the collection optics, while the fluence and length of the stripe must be varied for each data point. This restricts the accuracy of measurement based on the number of collected points and quality of alignment. Furthermore, when spin-coated films are studied, the signal must be collected from a smooth, cleaved edge of a substrate, which does not permit characterization over substrates or waveguide stacks that are not simple to cleave (for example, glass substrates or a multilayered LED stack). There is also a risk of sample degradation when it is exposed to air, which makes prolonged VSL measurements in ambient conditions difficult.

In this paper, we describe an alternative technique to measure the optically pumped net modal gain of an active material film (hereby referred to as the Scattered Emission Profile (SEP) method). The technique and gain fit are based on the same principle as that of the VSL method, where the intensity versus length is fitted to a propagating wave equation to extract the gain. But, contrary to the VSL method, where the signal is collected from the edge at multiple stripe lengths, the SEP method images ASE signal scattered from the surface, allowing an accurate estimation of the net modal gain in one single measurement, without need for re-alignment. In the subsequent sections, we describe the setup, the fitting equation and procedure to perform the measurement. We show how the extracted gain values depend on the choice of excitation stripe length and demonstrate the technique's applicability by performing multiple measurements on two different lead halide perovskite films which are fabricated using different processes. The technique is validated against the VSL method by measuring and comparing the net modal gain over a reference perovskite film. We conclude the manuscript with a critical discussion and comparison to the VSL technique.

Gain measurement set-up

Set-up

To measure the net gain of a sample, a 1-Dimensional gain-guided waveguide is created by impinging the active layer with a stripe shaped excitation. The intensity profile must be uniform along the stripe, and stripe width must be narrow[18,20] to promote longitudinally propagating modes. Figure 1(b) shows the normalized intensity profile of the pump stripe used in this work along the longitudinal axis (top) and the lateral axis (bottom).

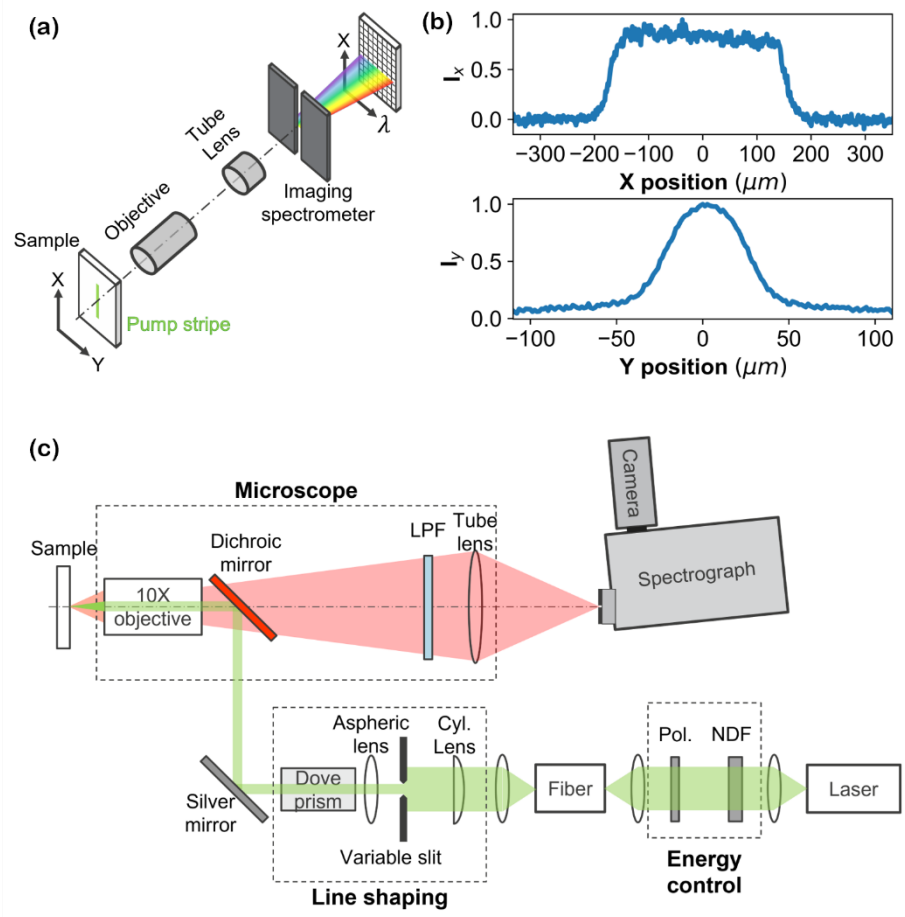

Fig. 1. (a) Schematic of alignment of excitation beam with imaging spectrometer, (b) intensity profile of excitation beam in the longitudinal and lateral axes, and (c) detailed setup schematic used in this paper.

Photoluminescence (PL) light emitted from the top of the sample is collected and projected onto the entrance slit of an imaging spectrometer using a microscope. The excitation stripe is oriented parallel to the entrance slit of the imaging spectrometer as shown in the sketch in Figure 1(a), and a detailed top-view schematic of our implementation of the setup is shown in Figure 1(c). The light entering the spectrograph is impinged on a 1D grating and imaged on a camera. The 1D grating preserves spatial information (such as PL intensity) along the longitudinal axis of the slit and spatially distributes light as a function of its wavelength along the lateral axis.

The PL emission collected from the surface is a summation of two components: a vertically outcoupled spontaneous emission and a fraction of the guided mode ASE contained within the waveguide, which is scattered out due to roughness-induced index variation. The optical gain of the film is extracted by analyzing the spatial profile of the scattered ASE signal. Thin film materials may sometimes contain strong scattering points such as voids which provide a strong index difference within the core of the waveguide. This is detrimental to extracting the gain because they introduce reflections to the guided mode and distort the spatial profile of the ASE (similar to the simulations performed by Wu et al[30]).

Due to the random nature of film roughness, the intensity of collected ASE is scaled by a random scattering loss which varies at different positions along the stripe. To reduce the effect

of relatively strong local scattering points and to get a smooth spatial ASE profile, the measurement is averaged over multiple physical locations on the sample. Figures 2(a,b) show the averaged PL spectra and optical Input-Output (IO) curve obtained for different pump fluences over our reference sample (120nm thick $MAPbI_3$ encapsulated by 100nm of PMMA, deposited on a Si/SiO_2 substrate). At low pump fluence, the PL spectra show a Gaussian shape, which is characteristic of the spontaneous emission released from the perovskite. As the pump fluence is increased, the spectra begin to show a second peak related to ASE around 790nm wavelength, which has a narrower linewidth and shows a steeper increase of intensity as a function of pump fluence compared to the spontaneous emission.

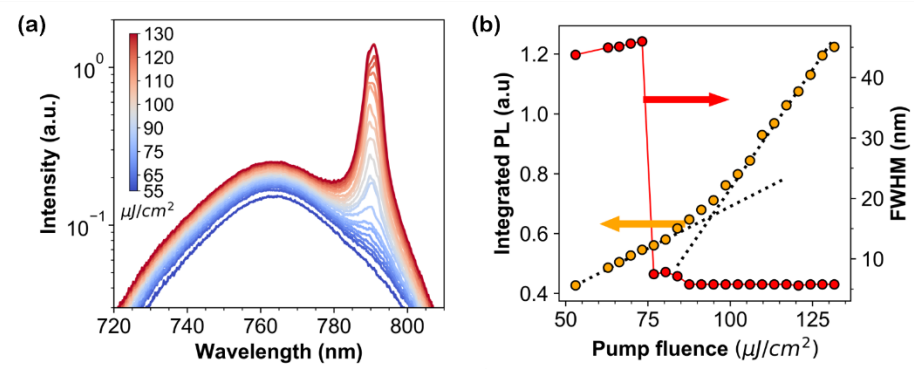

Fig. 2 (a) Averaged PL spectra collected at increasing pump fluence and (b) optical Input-Output curve. The (left) integrated energy and (right) Full Width Half Maximum (FWHM) linewidth of the PL spectra are plotted versus fluence.

The average near field spectrum recorded on the sample when it is pumped above threshold fluence is shown in Figure 3(a), where the y-axis represents the spatial position along the stripe from which scattered light is collected, and the x-axis represents the photon energy. In order to do quantitative analysis on the photon count, the spectra are displayed and processed in the energy axis rather than wavelength axis [31]. A spectrum from one of the rows on the image is shown in Figure 3(c). By subtracting a fitted Gaussian (black dashed line) from the PL spectrum and integrating the area under the curve over the gain bandwidth (as shown in the red shaded zone), the ASE intensity collected by the spectrometer at any point along the stripe can be calculated. This intensity is plotted as a function of position and is shown in Figure 3(d). Unlike the spontaneous emission, which is uniform along the excitation stripe, the ASE is much stronger at the ends of the stripe. This phenomenon occurs when light (emitted from the extreme ends of the stripe) experiences maximal amplification as it propagates along the entire length of the gain-guided waveguide. The intensity profile can be described using a fit equation (red dashed line in Figure 3(d)) which can be modelled as a sum of two counterpropagating amplified guided modes (as shown in Figure 3(d) as the Backward (BWD, dotted) and the Forward (FWD, dot-dashed) lines).

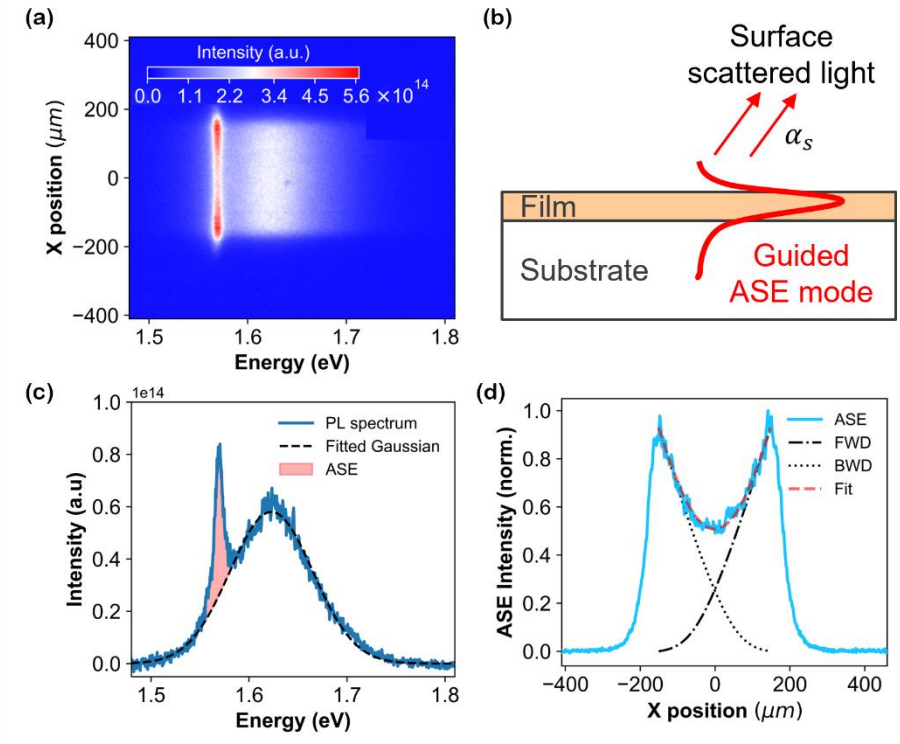

Fig. 3 (a) Averaged near-field spectrum of sample at pump fluence of 100uJ/cm^2, (b) sketch illustrating outcoupling of ASE light, (c) PL spectrum at one position along the stripe with red shaded area representing photon energy in ASE bandwidth, and (d) integrated ASE intensity along the excitation stripe with propagating wave fits.

Gain fit

As mentioned in the previous section, the ASE intensity profile is calculated by subtracting a fitted Gaussian spontaneous emission ($I_{sp}(x,\nu)$) from the measured spectrum ($I_{PL}(x,\nu)$) and integrating the area under the curve at every position along the stripe (described by equation (1)).

$$I_{ASE}(x) = \int^{\nu_{ASE}} \Big(I_{PL}(x,\nu) - I_{sp}(x,\nu)\Big) \cdot d\nu \tag{1}$$

The uni-directional propagation equation used to model the ASE intensity at any point of a waveguide is described in equation (2) [23]:

$$\frac{dI(x; g_0, I_{sat})}{dx} = \frac{g_0\, I(x)}{1 + \frac{I(x)}{I_{sat}}} + \frac{\beta}{1 + \frac{I(x)}{I_{sat}}} \cdot \Omega \tag{2}$$

Where g_0 is the small-signal net modal gain which is independent of intensity (henceforth referred to as net gain for brevity), I_{sat} is the saturation intensity, β is the spontaneous emission within the gain bandwidth inside the film (described in equation (3)), and Ω is the solid angle containing the strongest guided emission (described in equation (5)).

$$\beta = \frac{\int I_{sp}(x,\nu) \cdot d\nu}{dx \cdot \eta_{out}} \cdot \frac{\int^{\nu_{ASE}} I_{sp}(\nu) \cdot d\nu}{\int I_{sp}(\nu) \cdot d\nu} \tag{3}$$

$$\eta_{out} = \frac{1}{4\pi R^2} \int_{\phi=0}^{2\pi} \int_{\theta=0}^{\theta_{crit}} R^2 \, sin\theta \cdot d\theta \cdot d\phi = \frac{1}{2}(1 - \cos(\theta_{crit})) \quad (4)$$

η_{out} is the average fraction of power outcoupled from the surface by randomly oriented dipoles in the film (described in equation (4)), and θ_{crit} is the critical angle between the core and air. To account for the effect of waveguiding, the Ω term is calculated which describes the fraction of spontaneous emission emitted from one end of the stripe and travels up to the other end. Wave vectors corresponding to the furthest propagating rays in the waveguide stand the highest chance of being amplified and constitute the dominant outcoupled signal[23]. The angles considered for these equations are illustrated in Figure S1.

$$\Omega = \frac{1}{4\pi R^2} \int_{\phi=-\phi_1}^{\phi_1} \int_{\theta=\theta_{crit}}^{\pi-\theta_{crit}} R^2 \, sin\theta \cdot d\theta \cdot d\phi = \left[\frac{2}{\pi} \tan^{-1}\left(\frac{w_{1/e}}{2L}\right)\right] \cdot \Gamma_{gm} \quad (5)$$

$$\Gamma_{gm} = \left[\frac{1}{2}\cos\left(\theta_{crit,max}\right)\right] \quad (6)$$

Where $w_{1/e}$ is the stripe width, and L is the stripe length. The second term (Γ_{gm}) represents the fraction of intensity coupled from an isotropic dipole emitter to a 1D slab waveguide. The critical angle considered while calculating the coupling to the waveguide depends on the surrounding layers. Generally, the power contained within the highest critical angle is coupled to the guided mode.

The longitudinal intensity distribution of ASE intensity is described by summing two counterpropagating waves, described in equation (7).

$$F(x;\ g_0, I_{sat}) = \int_0^L \frac{dI(x; g_0, I_{sat})}{dx} \cdot dx + \int_L^0 \frac{dI(L-x; g_0, I_{sat})}{dx} \cdot dx \quad (7)$$

Equation (7) is used to model the spatial distribution of ASE (from equation (1)) by fitting the terms g_0 and I_{sat}, and the net gain is extracted from the best fit.

The terms describing the coupling of light out from the surface (η_{out}) and to the guided mode (Γ_{gm}) must be calculated by applying simulation techniques like Finite Difference Time Domain (FDTD) for a system where the thickness of the film is less than one wavelength.

Dependence on surface scattering loss

The equations described in the previous section are used to fit the intensity profile of ASE along the gain-guided waveguide. However, the previously calculated value of β can only be applied to the intensity of ASE inside the waveguide. In order to obtain an accurate fit, the ASE signal captured by the spectrometer must be scaled up by a random surface scattering loss (α_s) to reflect the true guided mode intensity inside the waveguide (Scaled Intensity = $I_{ASE}(x)/(\alpha_s \cdot dx)$). An approximate value for this loss can be determined by inspecting the near-field spectrum at threshold, when the net gain is close to zero. Under such a condition, stimulated emission can be observed in the spectrum, but it is uniformly distributed along the stripe. The spectrometer picks up a combination of vertically outcoupled PL and a small contribution from the guided mode in the ASE bandwidth, which can be isolated by subtracting the Gaussian spontaneous emission. By using the calculated value for β at threshold (β_{th}), the average scattering loss in the film can be determined using equation (8).

$$\alpha_s \cdot dx = \frac{I_{ASE,th}}{L\beta_{th}\Omega} \quad (8)$$

Where $I_{ASE,th}$ is the average collected intensity in the gain bandwidth at threshold and β_{th} is the spontaneous coupling at ASE threshold. The value obtained from equation (8) has no unit and must be used to scale the ASE intensity to perform gain fits. To obtain the scattering loss in units of cm^{-1}, the value obtained above must be divided by the step length 'dx'. Figure S2(b,c)

shows the collected ASE intensity at threshold and Figure S3 shows the collected intensity scaled up by the scattering loss described in the previous paragraph, along with the fitted (linear) forward and backward propagating waves at threshold.

Fitted Gain dependence on fluence and stripe length

The fitted net gains show that the amplification efficiency depends on the pump fluence. At fluences close to threshold, the net gain rises sharply as it overcomes the absorption and scattering losses, whereas at higher fluences, it increases at a slower rate.
When the stripe length is reduced, the ASE threshold tends to increase[32,33]. The net gain for shorter excitation lengths is also investigated and shown in Figure 4. Interestingly, the measured gain tends to be higher for shorter stripe lengths, as has also been observed in other systems where the gain was measured using the VSL method[34]. This makes the choice of stripe length an important consideration when comparing the gain across different materials or systems. For shorter stripe lengths, the waveguide is less encumbered with gain saturation. With fewer photons in the waveguide, the number of available carriers for the exponential amplification is greater, which results in a higher small signal gain measurement.

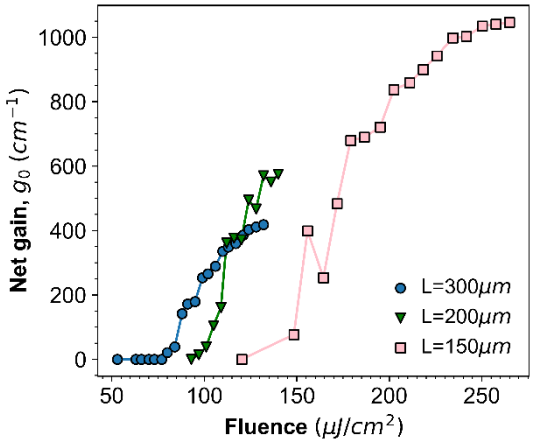

Fig. 4 Fitted net gain versus fluence for three different stripe lengths.

Reproducibility of SEP measurements

To verify the reproducibility of the SEP method, we perform additional gain measurements (using a fixed stripe length of 300 µm) over two other similar spin-coated $MAPbI_3$ films. Additionally, we perform SEP measurements on thermally evaporated $CsPbI_2Br$ films to demonstrate the wide applicability of the technique. Each $CsPbI_2Br$ film was annealed at 200°C for a duration of five seconds to improve its crystallinity. The PL spectra and ASE profiles (along with SEP fits) obtained from the first sample are shown in Figure S4. Figure 5 displays the extracted net modal gain for each sample under different pump fluences. For comparison, we include the reference $MAPbI_3$ sample ($MAPbI_3$-1) which was used in the previous sections.

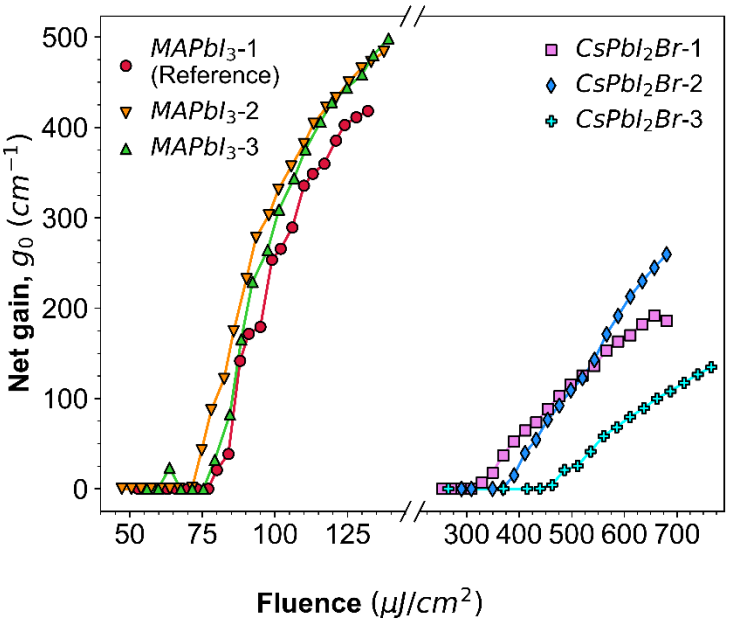

Fig. 5 Net modal gains extracted versus fluence for $MAPbI_3$ and $CsPbI_2Br$ samples.

The scattering losses for all the $MAPbI_3$ samples lay within the range of 7 cm^{-1} to 10 cm^{-1} (Figure S5(a)). Similar net modal gains are observed from the different samples, with minor differences arising due to process variability. While the surface scattering losses of the $CsPbI_2Br$ samples are lower than that of $MAPbI_3$ (varying between 2cm^{-1} to 4cm^{-1}, Figure S5(b)), they feature a significantly higher ASE threshold and lower net modal gains. Among the $CsPbI_2Br$ samples, the first two show similar ASE thresholds and comparable net modal gains whereas the third sample features a 50% higher ASE threshold and lower net modal gain. We attribute this difference in ASE threshold and gain performance to different crystallization conditions in the film arising due to process variations during the short annealing step.

Comparison of VSL measurement to SEP

To validate the SEP method, we compare the obtained gain values from the reference $MAPbI_3$ sample ($MAPbI_3$-1) to ones we measured with the VSL technique on the same sample. A similar setup as the one shown in Figure 1(c) was used, but the excitation stripe was rotated by 90 degrees (using the dove prism) and an optical fiber connected to the spectrometer was used to collect light from a cleaved sample edge. In the VSL approach, a unidirectional propagating wave equation (equation (2)) is used to fit the intensity collected from the edge using a fiber, using three values (g_0, β, and I_{sat}) as fitted parameters. The intensity collected from the edge using a fiber is plotted against the stripe length is shown in Figure 6(a) for fluences below and above threshold. Similarly, the average ASE profiles from multiple locations collected using the SEP method are plotted in Figure 6(b) for different fluences. The profiles measured at each location, and their corresponding net gains are shown in Figure S6. The fitted curves for both experiments are represented as black dashed lines in Figures 6(a) and (b), and the value of the fitted gains obtained using both techniques are shown in Figure 6(c). While the SEP fit produces very low fitting errors, uncertainties in the input values (such as stripe length, width, or material index) propagate into β and α_s, which can affect the fitted net gain value. By considering such input variations, the standard deviation of the fitted SEP net gain is calculated and displayed as the error bars in Figure 6(c).

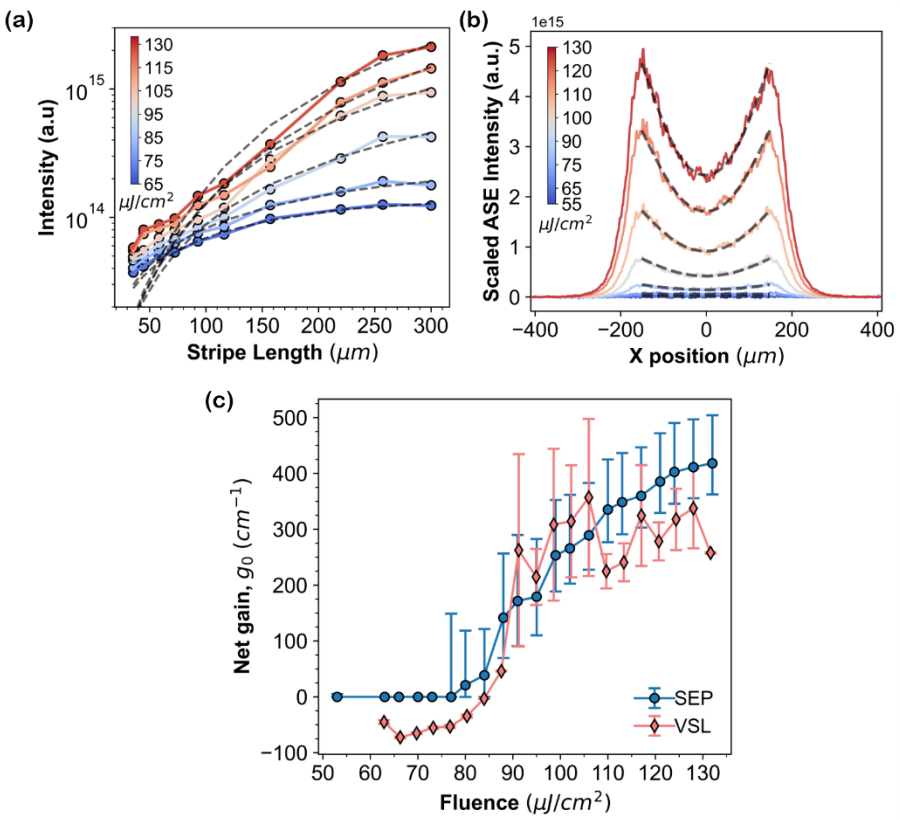

Fig. 6 (a) Intensity versus length obtained for VSL measurements at different pump fluences and saturation gain fit (black dashed lines), (b) averaged scaled ASE profiles ($I_{ASE}/(\alpha_s \cdot dx)$) obtained for increasing pump fluences and gain fit (black dashed lines), and (c) fitted gain versus fluence for VSL and SEP methods.

The VSL gain fit values are less than zero close to the threshold but approach the SEP fit above threshold. The fitted values also follow a similar trend as the SEP method: the gain rises sharply near threshold and slower at higher fluences. The agreement between the values obtained by the two methods is lower at higher fluences due to the limited resolution and varying collection efficiency for different stripe lengths in the VSL method.

Having used both techniques to extract the optical gain of our perovskite film, we have listed the corresponding advantages and disadvantages of both techniques in Table 1.

Table 1. Comparison of SEP and VSL methods

SEP	VSL
- Absolute value of ASE intensity is scaled by calculated scattering loss	+ ASE intensity is captured directly (if a clean cleaved edge can be created)
+ Single shot experiment	- Repeated measurements for each data point of stripe length and fluence
+ Easier setup alignment	- More careful alignment of beam to sample and sample to fiber from edge is required
+ Compatible with scaled LED stacks	- Requires measurement from cleaved edge, which is more difficult to achieve on LED

	stacks and films on amorphous substrates such as glass, polyimide, etc..
+ Greater fit accuracy with many more points	- Increasing the accuracy is at the expense of much longer measurement duration due to individual collection of signals at each stripe length
Fits with 2 parameters ('g_0', 'I_{sat}'), relies on calculating 'η_{out}', 'Γ_{gm}' and calculation of 'α_s'.	Fits with 3 parameters ('g_0', 'I_{sat}' and 'β') with no assumptions.

Conclusion

In this paper, the Scattered Emission Profile method is introduced as an alternative to enable a rapid measurement of the optical net modal gain of an active material. As highlighted in previous sections, this method relies on measuring the profile of scattered ASE light from the surface of an excited stripe. As long as the surface scattering is relatively uniform and weak (without inducing strong back-scattering of a propagating mode), the spatial profile of the ASE can be probed. A propagating mode equation is fitted to an integrated ASE profile, with the small-signal net modal gain and saturation intensity set as fitting parameters and the other values such as spontaneous emission coupled to the mode, outcoupling and scattering loss are calculated from the near-field spectra. With the elimination of the condition of edge measurement, this technique can be used to measure net gain directly for full LED structures or films on substrates which are not trivial to cleave, such as sapphire. The fitted gain numbers depend on the calculated average surface scattering loss, the choice of fluence, and stripe length. The experiment is performed on multiple copies of different films to show reproducibility of measurement and its broad applicability to different thin film gain media. Finally, the technique is compared to a VSL measurement which showed similar gain numbers close to threshold, and the pros and cons of both techniques are highlighted.

Set-up description

Figure 1(c) shows the set-up. The excitation laser used in this study is a CryLaS FTSS 355-300, whose 1064nm emission is frequency doubled using a nonlinear crystal to produce 532nm wavelength 3ns pulses at a repetition rate of 20Hz. The beam is attenuated using a combination of a variable neutral density filter and a polarizer and is focused into a multimode fiber to relocate the output pulse at any point on the optical table. An initial stripe excitation is created on a mechanical slit by imaging the fiber using an aspheric lens (f=50mm) and focusing the resulting beam along one axis using a cylindrical lens (f=50mm). Excitation uniformity is achieved by widening the Gaussian beam profile and impinging the central area of the excitation on the variable mechanical slit, which cuts off the tails of the beam and controls the length of the stripe (X axis in Figure 1(a,b)). This initial stripe excitation is subsequently imaged using an aspheric lens (f=100mm) and its orientation is controlled using a rotating dove prism. A dichroic mirror (Thorlabs DMLP567) placed in the optical axis of the microscope reflects the rotated beam into an objective (Mitutoyo 10X infinity corrected objective, f=20mm), which creates a 5X downsized image of the initial stripe excitation on the sample. The PL generated from this excitation was imaged using the same microscope objective combined with a 200mm tube lens and was focused on the entrance slit of an Imaging Spectrometer (SpectraPro HRS-500) and recorded with a PI-MAX 4 digital intensified camera. A 600nm long pass filter (LPF) was placed in the microscope axis to block any residual intensity from the pump laser.

Sample preparation

An equimolar mixture of perovskite precursor salts, MAI (CH_3NH_3I) and PbI_2, was dissolved in the N,N-dimethylformamide (DMF) to obtain 1.2M solution. The dilution was later adjusted to obtain 120nm thick $MAPbI_3$ films by a one-step spin-coating. $MAPbI_3$ precursor solution was spin-coated at 6000rpm for 34 seconds and the wet film was quenched by dropping 150µl of toluene four seconds after the start of the spinning. The film was annealed at 70°C for five minutes. To protect the film from degradation during ambient optical measurement using the VSL method, polymethyl methacrylate (PMMA) (40mg/ml in chlorobenzene) was spin-coated above the perovskite at 4000rpm for 60 seconds without sequential annealing.
The films were fabricated on a Si/SiO_2 substrate which were subsequently cleaved to produce a uniform thickness waveguide with a smooth edge. The thickness of the SiO_2 was around 1000nm (created by thermal oxidation) to isolate the perovskite mode from the substrate.

$CsPbI_2Br$ thin films were thermally evaporated from CsBr (abcr, ultra dry; 99.9%) and PbI_2(TCI Chemicals, >98%) precusrors using a Kurt J. Lesker SPECTROS system. The evaporation rates were calibrated with the use of spectroscopic ellipsometry and were set at 0.32 Å/s and 0.47 Å/s for CsBr and PbI_2, respectively, aiming at a 1.05:1.00 CsBr to PbI_2 molar ratio. The duration of the deposition was tuned to obtain 275 nm thick layers of $CsPbI_2Br$. To improve the deposition uniformity, the sample holder (loaded with nine 3 × 3 cm^2 glass substrates) was continuously rotating. After deposition, the samples were flash-annealed inside a glovebox at 200°C for approximately five seconds in order to improve their crystallinity.

Acknowledgement

The authors acknowledge funding from the European Research Council under the European Horizon 2020 Programme/ERC grant agreement no. 835133 (ULTRA-LUX).

Conflict of Interest

The authors declare no conflict of interest.

Data Availability Statement

The data that support the findings of this study are available from the corresponding authors upon reasonable request.

Funding Sources

The authors acknowledge funding from the European Research Council under the European Horizon 2020 Programme/ERC grant agreement no. 835133 (ULTRA-LUX).

Notes

The authors declare no competing financial interest.

Supporting Information

Supporting information available: Illustrations of angles and dimensions considered for calculations; Analysis of ASE at threshold to determine average scattering loss; PL spectra and spatial ASE profiles of a $CsPbI_2Br$ sample; Surface scattering loss estimates of $MAPbI_3$ and $CsPbI_2Br$ samples; Spatial ASE profiles and fitted gains at individual locations on $MAPbI_3$ sample-1; Spatial spontaneous emission profiles of $MAPbI_3$ sample-1.

References

(1) Quan, L. N.; Rand, B. P.; Friend, R. H.; Mhaisalkar, S. G.; Lee, T. W.; Sargent, E. H. Perovskites for Next-Generation Optical Sources, *Chem. Rev.* **2019**, 119, 12, 7444–7477. https://doi.org/10.1021/acs.chemrev.9b00107.
(2) Park, Y. S.; Roh, J.; Diroll, B. T.; Schaller, R. D.; Klimov, V. I. Colloidal Quantum Dot Lasers. *Nat Rev Mater*, **2021**, 6, 382–401. https://doi.org/10.1038/s41578-020-00274-9.
(3) Tessler, N. Lasers Based on Semiconducting Organic Materials. *Adv. Mater.*, **1999**, *11* (5), 363–370. https://doi.org/10.1002/(SICI)1521-4095(199903)11:5<363::AID-ADMA363>3.0.CO;2-Y.
(4) Roh, K.; Zhao, L.; Gunnarsson, W. B.; Xiao, Z.; Jia, Y.; Giebink, N. C.; Rand, B. P. Widely Tunable, Room Temperature, Single-Mode Lasing Operation from Mixed-Halide Perovskite Thin Films. *ACS Photonics*, **2019**, *6* (12), 3331–3337. https://doi.org/10.1021/acsphotonics.9b01501.
(5) Pourdavoud, N.; Mayer, A.; Buchmüller, M.; Brinkmann, K.; Häger, T.; Hu, T.; Heiderhoff, R.; Shutsko, I.; Görrn, P.; Chen, Y.; Scheer, H. C.; Riedl, T. Distributed Feedback Lasers Based on MAPbBr3. *Adv. Mater. Technol.*, **2018**, *3* (4). https://doi.org/10.1002/admt.201700253.
(6) Park, H.; Alasvand Yazdani, S.; Bencheikh, F.; Komatsu, R.; Yokoyama, S.; Kamiya, T.; Adachi, C. Control of Emission Diffraction Angles and Laser Threshold in Mixed-Order Sampled Distributed Feedback Laser with Organic Gain Media. *J. Appl. Phys.*, **2022**, *132* (20). https://doi.org/10.1063/5.0123476.
(7) Whitworth, G. L.; Dalmases, M.; Taghipour, N.; Konstantatos, G. Solution-Processed PbS Quantum Dot Infrared Laser with Room-Temperature Tunable Emission in the Optical Telecommunications Window. *Nat. Photonics*, **2021**, *15* (10), 738–742. https://doi.org/10.1038/s41566-021-00878-9.
(8) Cho, C.; Palatnik, A.; Sudzius, M.; Grodofzig, R.; Nehm, F.; Leo, K. Controlling and Optimizing Amplified Spontaneous Emission in Perovskites. *ACS Appl. Mater. Interfaces*, **2020**, *12* (31), 35242–35249. https://doi.org/10.1021/acsami.0c08870.
(9) Zhu, Y.; Xie, W.; Bisschop, S.; Aubert, T.; Brainis, E.; Geiregat, P.; Hens, Z.; van Thourhout, D. On-Chip Single-Mode Distributed Feedback Colloidal Quantum Dot Laser under Nanosecond Pumping. *ACS Photonics*, **2017**, *4* (10), 2446–2452. https://doi.org/10.1021/acsphotonics.7b00644.
(10) Goldberg, I.; Qiu, W.; Elkhouly, K.; Annavarapu, N.; Mehta, A. N.; Rolin, C.; Ke, T.-H.; Gehlhaar, R.; Genoe, J.; Heremans, P. Active Area Dependence of Optoelectronic Characteristics of Perovskite LEDs. *J. Mater. Chem. C,* **2021**, *9, 12661-12670.* https://doi.org/10.1039/D1TC03138D.
(11) Elkhouly, K.; Goldberg, I.; Annavarapu, N.; Gehlhaar, R.; Ke, T. H.; Genoe, J.; Hofkens, J.; Heremans, P.; Qiu, W. Intense Electrical Pulsing of Perovskite Light Emitting Diodes under Cryogenic Conditions. *Adv. Opt. Mater.*, **2022**, *10* (15). https://doi.org/10.1002/adom.202200024.
(12) Zhao, L.; Roh, K.; Kacmoli, S.; al Kurdi, K.; Liu, X.; Barlow, S.; Marder, S. R.; Gmachl, C.; Rand, B. P. Nanosecond-Pulsed Perovskite Light-Emitting Diodes at High Current Density. *Adv. Mater.*, **2021**, *33* (44). https://doi.org/10.1002/adma.202104867.
(13) Ahn, N.; Park, Y.; Livache, C.; Du, J.; Gungor, K.; Kim, J.; Klimov, V. I. Optically Excited Lasing in a Cavity-Based, High-Current-Density Quantum Dot

Electroluminescent Device. *Adv. Mater.*, **2023**, 2206613. https://doi.org/10.1002/adma.202206613.

(14) Cegielski, P. J.; Giesecke, A. L.; Neutzner, S.; Porschatis, C.; Gandini, M.; Schall, D.; Perini, C. A. R.; Bolten, J.; Suckow, S.; Kataria, S.; Chmielak, B.; Wahlbrink, T.; Petrozza, A.; Lemme, M. C. Monolithically Integrated Perovskite Semiconductor Lasers on Silicon Photonic Chips by Scalable Top-Down Fabrication. *Nano Lett.*, **2018**, *18* (11), 6915–6923. https://doi.org/10.1021/acs.nanolett.8b02811.

(15) Kallinger, C.; Hilmer, M.; Haugeneder, A.; Perner, M.; Spirkl, W.; Lemmer, U.; Feldmann, J.; Scherf, U.; Muellen, K.; Gombert, A.; Wittwer, V. A Flexible Conjugated Polymer Laser. *Adv. Mater.* **1998**, *10* (12), 920–923. https://doi.org/10.1002/(SICI)1521-4095(199808)10:12<920::AID-ADMA920>3.0.CO;2-7.

(16) Mathies, F.; Brenner, P.; Hernandez-Sosa, G.; Howard, I. A.; Paetzold, U. W.; Lemmer, U. Inkjet-Printed Perovskite Distributed Feedback Lasers. *Opt. Express*, **2018**, *26* (2), A144. https://doi.org/10.1364/OE.26.00A144.

(17) Dong, Pu-Ting, and Ji-Xin Cheng. Pump–probe microscopy: theory, instrumentation, and applications [Online]. *Spectroscopy*, **2017**, 32.4, 24-36. https://www.spectroscopyonline.com/view/pump-probe-microscopy-theory-instrumentation-and-applications (accessed Dec 1, 2022).

(18) Shaklee, K. L.; Nahory, R. E.; Leheny, R. F. Optical Gain in Semiconductors. *J. Lumin.*, **1973**; Vol. 7, 284-309. https://doi.org/10.1016/0022-2313(73)90072-0.

(19) Valenta, J.; Luterová, K.; Tomasiunas, R.; DohnalovÁ, K.; Hönerlage, B.; Pelant, I. Optical Gain Measurements With Variable Stripe Length Technique. *Towards the First Silicon Laser*, **2003**, 93, pp 223–242.

(20) Cross, P. S.; Oldham, W. G. Theory of Optical-Gain Measurements. *IEEE J. Quantum Electron.*, **1975**, *11* (5), 190–197. https://doi.org/10.1109/JQE.1975.1068592.

(21) Cross, P. S.; Oldham, W. G. Monolithic Measurement of Optical Gain and Absorption in PbTe. *J. Appl. Phys.*, **1975**, *46* (2), 952–954. https://doi.org/10.1063/1.321624.

(22) Blood, P.; Lewis, G. M.; Smowton, P. M.; Summers, H.; Thomson, J.; Lutti, J. Characterization of Semiconductor Laser Gain Media by the Segmented Contact Method. *IEEE J. Sel. Top. Quantum Electron.*, **2003**, Vol. 9, pp 1275–1282. https://doi.org/10.1109/JSTQE.2003.819472.

(23) Dal Negro, L.; Bettotti, P.; Cazzanelli, M.; Pacifici, D.; Pavesi, L. Applicability Conditions and Experimental Analysis of the Variable Stripe Length Method for Gain Measurements. *Opt. Commun.*, **2004**, *229* (1–6), 337–348. https://doi.org/10.1016/j.optcom.2003.10.051.

(24) Lange, C.; Schwalm, M.; Chatterjee, S.; Rühle, W. W.; Gerhardt, N. C.; Johnson, S. R.; Wang, J. B.; Zhang, Y. H. The Variable Stripe-Length Method Revisited: Improved Analysis. *Appl. Phys. Lett.*, **2007**, *91* (19). https://doi.org/10.1063/1.2802049.

(25) Xing, G.; Mathews, N.; Lim, S. S.; Yantara, N.; Liu, X.; Sabba, D.; Grätzel, M.; Mhaisalkar, S.; Sum, T. C. Low-Temperature Solution-Processed Wavelength-Tunable Perovskites for Lasing. *Nat. Mater.*, **2014**, *13* (5), 476–480. https://doi.org/10.1038/nmat3911.

(26) Alvarado-Leaños, A. L.; Cortecchia, D.; Folpini, G.; Srimath Kandada, A. R.; Petrozza, A. Optical Gain of Lead Halide Perovskites Measured via the Variable Stripe Length

Method: What We Can Learn and How to Avoid Pitfalls. *Adv. Opt. Mater.*, **2021**, *9* (18). https://doi.org/10.1002/adom.202001773.

(27) Yakunin, S.; Protesescu, L.; Krieg, F.; Bodnarchuk, M. I.; Nedelcu, G.; Humer, M.; de Luca, G.; Fiebig, M.; Heiss, W.; Kovalenko, M. v. Low-Threshold Amplified Spontaneous Emission and Lasing from Colloidal Nanocrystals of Caesium Lead Halide Perovskites. *Nat. Commun.*, **2015**, *6*. https://doi.org/10.1038/ncomms9056.

(28) Sutherland, B. R.; Hoogland, S.; Adachi, M. M.; Kanjanaboos, P.; Wong, C. T. O.; McDowell, J. J.; Xu, J.; Voznyy, O.; Ning, Z.; Houtepen, A. J.; Sargent, E. H. Perovskite Thin Films via Atomic Layer Deposition. *Adv. Mater.*, **2015**, *27* (1), 53–58. https://doi.org/10.1002/adma.201403965.

(29) Geiregat, P.; Maes, J.; Chen, K.; Drijvers, E.; de Roo, J.; Hodgkiss, J. M.; Hens, Z. Using Bulk-like Nanocrystals To Probe Intrinsic Optical Gain Characteristics of Inorganic Lead Halide Perovskites. *ACS Nano*, **2018**, *12* (10), 10178–10188. https://doi.org/10.1021/acsnano.8b05092.

(30) Wu, X.; Andreasen, J.; Cao, H.; Yamilov, A. Effect of Local Pumping on Random Laser Modes in One Dimension. *J. Opt. Soc. Am. B*, **2007**, 24, A26-A33. https://doi.org/10.1364/JOSAB.24.000A26.

(31) Mooney, J.; Kambhampati, P. Get the Basics Right: Jacobian Conversion of Wavelength and Energy Scales for Quantitative Analysis of Emission Spectra. *J. Phys. Chem. Lett.*, **2013**, 4, pp 3316–3318. https://doi.org/10.1021/jz401508t.

(32) Peters, G. I.; Allen, L. Amplified Spontaneous Emission I. The Threshold Condition. *J. Phys. A: Gen. Phys.*, **1971**, Vol. 4, 238. https://doi.org/10.1088/0305-4470/4/2/009.

(33) Belitsch, M.; Dirin, D. N.; Kovalenko, M. v.; Pichler, K.; Rotter, S.; Ghalgaoui, A.; Ditlbacher, H.; Hohenau, A.; Krenn, J. R. Gain and Lasing from CdSe/CdS Nanoplatelet Stripe Waveguides. *Micro and Nano Engineering*, **2022**, *17*. https://doi.org/10.1016/j.mne.2022.100167.

(34) Guzelturk, B.; Pelton, M.; Olutas, M.; Demir, H. V. Giant Modal Gain Coefficients in Colloidal II-VI Nanoplatelets. *Nano Lett.*, **2019**, *19* (1), 277–282. https://doi.org/10.1021/acs.nanolett.8b03891.

For Table of Contents Use Only

Table of Contents Graphic

Scattered Emission Profile Technique for Accurate and Fast Assessment of Optical Gain in Thin Film Lasing Materials

NIRAV ANNAVARAPU, IAKOV GOLDBERG, ATHINA PAPADOPOULOU, KARIM ELKHOULY, JAN GENOE, ROBERT GEHLHAAR, PAUL HEREMANS

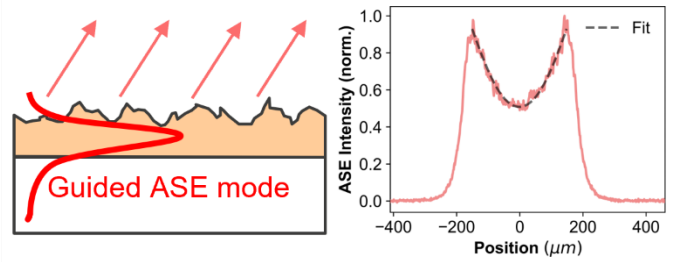

ASE light scattered out from a waveguide can be analyzed to extract net modal gain of a thin film material